Development of Green MMT-modified Hemicelluloses Based Nanocomposite Film with Enhanced Functional and Barrier Properties

Kassim M. Haafiz,[a,*] Owolabi F. A. Taiwo,[a,b] Nadhilah Razak,[a] Hashim Rokiah,[a] Hussin M. Hazwan,[c] Nurul Fazita M. Rawi,[a] and H. P. S. Abdul Khalil [a]

A biocomposite was successfully prepared by blending montmorillonite (MMT)/hemicellulose from oil palm empty fruit bunches (OPEFB) with carboxymethyl cellulose (CMC) through solution casting. The composite was characterized by scanning electron microscopy (SEM), Fourier transmission infrared spectroscopy (FT-IR), and X-ray diffraction (XRD). The results displayed good compatibility between the mixtures of the blended MMT/hemicellulose and CMC due to the hydrogen bonding and electrostatic interaction. There was an improvement in the thermal analysis through their thermogravimetry analysis (TGA), derivative thermogravimetry (DTG), and differential scanning calorimetry (DSC), mechanical properties (tensile strength and tensile modulus),and water vapor permeability (WVP). The best values of tensile strength and tensile modulus of 47.5 MPa and 2.62 MPa, respectively, were obtained from 60H-40CMC-MMT nanocomposite films. The results showed that the mixture of the blended MMT/hemicelluloses and CMC produced a robust nanocomposite film with improved physical and mechanical properties, demonstrating that it is a promising candidate for green packaging applications.

Keywords: Oil palm empty fruit bunch; Montmorillonite; Hemicelluloses; Solution casting; Carboxymethyl cellulose

*Contact information: a: Bioresource, Paper and Coatings Technology Department, School of Industrial Technology, Universiti Sains Malaysia, 11800 Penang, Malaysia; b: Pulp and Paper division of Chemical, Fibre and Environmental Technology Department Federal Institute of Industrial Research Oshodi, Nigeria; c: Lignocellulosic & Materials Technology Research Group, School of Chemical Sciences, Universiti Sains Malaysia, 11800 Minden, Penang, Malaysia; *Corresponding author: mhaafiz@usm.my*

INTRODUCTION

Hemicellulose is made of alkali-soluble, biodegradable, biocompatible, natural hetero-polysaccharides that have limited utilization in packaging due to their hygroscopicity and poor mechanical properties (Chen *et al*. 2016). Global demand for high-barrier food-packaging films was reported to have increased from 2015 to 1.4 million tons in 2017, which is equivalent to USD 230.97 billion. This is expected to rise at a compound growth rate (CAGR) of 7.8% between 2017 and 2027, valued as US$430.08 billion by 2027 (Aldaya *et al*. 2010). The increase in the demand for green packaging materials, especially in food packaging, is a reflection of changing lifestyles with respect to the convenience and portability of products from the food industry (Nasrabadi *et al*. 2017). The basic properties that make good packaging materials include chemical properties, heat resistance, odor barrier, puncture resistance, high tensile strength, durability, good surface properties, and low weight, and these factors have contributed to the growing requirements

of the food industry and retail supply chain (Luqueta *et al*. 2017). The application of renewable resources such as plant materials in packaging are expected to reduce the dependence on fossil fuel materials for packaging. Of the three principal biopolymers in plants, hemicellulose has received the least attention in terms of application. While cellulose has a unique structure, the term hemicelluloses is used to describe a number of noncrystalline hexose and pentose sugars (Andberg *et al*. 2016). Hemicelluloses make up 20 to 30% of the total weight of perennial and annual plants; they are abundant polysaccharides with good film forming ability and excellent oxygen and water vapor barrier properties. The composition of hemicellulose depends on the method of its extraction, *i.e*. by steam, alkali, methanol/water, dimethyl sulfoxide, or microwave (Chaker *et al*. 2013). Hemicelluloses are often released to the stream during forest operations such as pulping, disposed as an organic waste, burned for energy recovery, or released during fiberboard production, and these materials could be used as renewable resources for packaging materials. Hemicellulose-based films have been used as barrier materials for moisture and oxygen and in the production of polarizing sheets (Creighton *et al*. 2016). The mechanisms of hemicelluloses reactions as bio-fillers are influenced by the variability in sugar constituents, glycosidic linkages, structure of glycosyl side chains, and the reactive hydroxyl groups at the xylose repeating unit (Reza *et al*. 2013). These linkages offer various possibilities for region-selective chemical and enzymatic modifications. These and other applications motivate an interest in improving various properties of hemicellulose by blending with other polymeric materials. The abundant hydroxyl groups in hemicelluloses makes it hydrophilic, and it can participate in intermolecular and intramolecular hydrogen bonding. However, hemicellulose-based films are hygroscopic with poor mechanical strength properties (Chen *et al*. 2016). To overcome these disadvantages, plasticizers such as carboxymethyl cellulose (CMC) and xylitol are often introduced to the composite blend (Chen *et al*. 2016).

Carboxymethyl cellulose is a cellulose derivative that is prepared through the reaction of alkali cellulose with mono-chloro acetate or its sodium salt in organic medium. It possesses many desirable qualities, such as film forming, emulsification, stabilization of suspensions, water retention, binding, and thickening. Therefore, it is used for many applications such as in medicine, food, textures, toilet, electrical elements, papermaking, printing, and dying. There are many potential applications of CMC in paper coating, textile sizing, and flexible water-soluble packing film due to its high clarity and excellent durability. The mechanical strength properties of a polysaccharide film can be increased by blending with a higher molecular weight polysaccharide that has adhesive properties, such as CMC. It shows amphiphilic characteristics due to the presence of many hydrophilic carboxyl groups (Yu *et al*. 2014). The most popular bentonites are montmorillonite (MMT), hectorite, and saponite. Of these, MMT is the most widely used clay as nanofiller for CMC modification due to its availability in many localities (Makwana *et al*. 2018).

Despite the various literature reports on the fabricated hemicellulose based biodegradable films, practical applications of hemicelluloses films have been severely limited. Zhao and coworkers (2015) further reported that, combination of hemicellulose and plasticizer based nanocomposite films often aimed to ensure enhanced functional properties has rarely been investigated. The aim of this study is to prepare high performance green hemicelluloses based nanocomposite film from the blend of montmorillonite (MMT)/ hemicellulose from oil palm empty fruit bunches (OPEFB) with carboxyl methyl cellulose (CMC). To date, packaging film from extracted hemicelluloses from oil palm empty fruit bunches (OPEFB) fortified with montmorillonite has not been

reported with respect to film forming and barrier characterization. The present study developed and characterized eco-friendly biodegradable film from waste OPEFB with improved functional and good barrier properties for low to moderate relative humidity applications.

EXPERIMENTAL

Materials

The raw materials used to produce the nanocomposite films were carboxymethyl cellulose (Drex-Chem (M) Sdn. Bhd., Petaling Jaya, Selangor, Malaysia) and organo-modified montmorillonite (Nanocor Inc., Arlington Heights IL, USA). Hemicellulose from oil palm empty fruit bunch (OPEFB) was supplied by United Oil Palm Sdn Bhd, Nibong Tebal, Penang, Malaysia.

Hemicellulose Extraction from of Oil Palm Empty Fruit Bunch

Alkaline extraction was performed as described by Wanrosli *et al*. (2004) with the modification of using NaOH instead of KOH. The hemicellulose extraction was conducted at the biomass to alkaline ratio of 1:10 (wt:vol). The total weight of 5 g OPEFB was placed in a beaker with 50 mL of 1.0 M NaOH. The beaker was heated at 40 °C on a magnetic stirrer for 4 h at 400 rpm. The mixture was refrigerated for 24 h at 4 °C. The supernatant was collected, and hemicellulose was precipitated by adding ethanol.

Hemicelluloses Based Film Preparation

This process was repeated two times. The extracted hemicellulose was separated from residue by filtration. The hemicellulose-based composites were reconstituted with 20%, 40%, 60%, or 80% hemicelluloses, which were denoted as 20H-80CMC, 40H-60CMC, 60H-40CMC, and 80H-20CMC, respectively, where 100CMC was used as the control (Table 1).

Table 1. Formulation for Nanocomposite Film

Sample	Hemicellulose (%)	CMC (%)
100CMC	0	100
20H-80CMC-MMT	20	80
40H-60CMC-MMT	40	60
60H-40CMC-MMT	60	40
80H-20CMC-MMT	80	20
Note: To produce nanocomposite film, 2% of MMT was added to the blend film		

Initially, a distilled water solution of hemicelluloses was transferred into a beaker, followed by additional of CMC, at 90 °C for 30 min under moderate agitation as shown in Table 1. Finally, the film solution was transferred into poly-acrylic plates and drying in an oven (Mermet, Germany) at 45 ± 0.5 °C and relative humidity of 60% for 36 h to obtain a film of uniform thickness. All of the produced films were placed inside a desiccator containing silica-gel prior to analysis.

Characterization

Film thickness

Film thickness was measured using a hand-held micrometer (Mitutoyo, Tokyo, Japan) to the nearest 0.001 mm at twelve different locations, and the average value was obtained. The thickness was used in the calculations for film water vapor permeability and mechanical properties of the films.

Contact angle analysis

Contact angles were measured to study the surface hydrophobicity of the films. The contact angle analysis was determined using a Drop Shape Analyzer DSA100 goniometer (Kruss GmbH, Hamburg, Germany), which is a universal, high-quality instrument for analyzing wetting and coating processes. The wettability test was carried out using water, where10 µL of water was dropped manually using a micropipette onto the surface of the particleboard. The image of the droplet was recorded using video camera for 60 s. Five replicates were used for the determination of contact angle for each liquid.

Fourier transform infrared analysis (FTIR)

Fourier transform infrared (FTIR) spectroscopy of hemicelluloses film from blend of CMC, MMT, and OPEFB and nanocomposite were measured directly using a Nicolet Avatar Model 360 spectrometer Fourier transform infrared spectrometer (Thermo Nicolet Corporation, Madison, WI, USA). FT-IR spectra were recorded in the spectra range from 4000 to 400 cm^{-1}. The spectra were recorded in the absorbance mode at from 4000 to 400 cm^{-1} by FTIR analysis immediately afterward.

X-ray diffraction analysis

The X-ray diffraction (XRD) patterns of the hemicelluloses film were obtained on a Philips PW1050 X-pert diffractometer (Radeberg, Germany) using Cu-Ka1 radiation and operation at 40 kV and 25 Ma and λ = 1.54 Å. The diffractrograms were scanned from 1° to 60° (2θ) in steps of 0.02° using a scanning rate of 0.5°C/min. X-ray diffractograms of hemicelluloses film was carried out for determining the degree of crystalline or amorphous nature of the samples, chemical composition of raw material and particle size. The diffractometer was controlled by a personal computer equipped with X-pert High Score puls Software. 2 g of samples from hemicelluloses nanocomposite film were used prior to analysis.

Water vapor permeability

Water vapor permeability (WVP) of the film sample was measured using ASTM D570-98 (2002). The film sample was mounted on a permeation glass cup (height of 410 mm; width of 450 mm) containing silica gel. The initial weight of the cup together with the film sample and silica gel was recorded before putting in a desiccator containing a beaker of water kept at 25±2°C. The cup was weighed (±0.0001 g) daily for a week, and a plot of weight gained against time was drawn. According to Jouki *et al*. (2013), the water vapor transmission rate (WVTR) and WVP were calculated using Eqs. 1 and 2,

$$WVTR = \Delta m/\Delta t A \quad (1)$$

$$\text{WVP=WVTR } (L/\Delta p) \quad (2)$$

where $\Delta m/\Delta t$ is the moisture gain weight per time (g/s), A is the exposed surface area of

the film (m^2), L is the thickness of the film (mm), and Δp is the difference of partial pressure.

Tensile Strength

Film samples of each formulation was uniformly cut into strips (150 mm × 25 mm), and tensile strength (TS), Young's modulus (E), and elongation at break (EAB) was measured and calculated according to ASTM D882 (2000) using a texture analyzer (Stable Micro Systems TA.XT plus, Surrey, UK). The film strip was clamped between tensile grips with an initial grip separation and test speed set at 100 mm and 0.8 mm s^{-1}, respectively, using a load cell of 30 kg. For each sample, the film was cut, and an average of five measurements was taken to calculate TS, E, and EAB according to the following equations,

$$\text{TS (MPa)} = F_{max} / Ø \quad (3)$$

$$\text{E (MPa)} = (F_{max} / Ø) \times (l_O / \Delta l) \quad (4)$$

$$\text{EAB (\%)} = (\Delta l / l_O) \times 100 \quad (5)$$

where $F_{max}$is the maximum load (N), $Ø$ is the cross-sectional area of the film strips (mm^2), l_O is the initial film length (mm), and Δl is the length of film extension after stretching (mm).

Scanning Electron Microscopy (SEM)

The morphology of the blend and nanocomposites film was investigated with a scanning electron microscope (Leo Supra, 50 VP, Carl Ziess, SMT, Radeberg, Germany). Images were obtained under conventional secondary electron imaging. The fracture surfaces of composites obtained from tensile fracture cross sections were sputter-coated with gold prior to microscopy.

Thermal Analysis

Differential scanning calorimetry (DSC)

A Perkin Elmer Pyris 7 thermal analyzer (Radeberg, Germany) was utilized to determine the melting temperature for hemicellulose film under nitrogen purge at a heating hate of 10 °C/min. Approximately 10 mg of dry sample was transferred into a hermetic aluminum pan and sealed. The sample was placed inside the analyzer with an empty hermetic aluminum pan as reference. The sample was heated at 10°C/min in nitrogen flux from room temperature to 400 °C. The data was recorded continuously over the temperature and time intervals. As the temperature increased, the sample eventually reached its melting temperature (T_m). The melting process resulted in an endothermic peak in the DSC curve.

Thermogravimetric analysis (TGA)

Thermogravimetric analysis was used to evaluate the thermal stability of hemicellulose film specimens. The weight loss of the samples was measured as a function of temperature using a thermogravimetric analyzer (Perkin-Elmer) under nitrogen atmosphere at a flow rate of 20 mL/min. A total of 10 mg of dried sample was heated at 10 °C/min in nitrogen flux from room temperature to 800 °C using Perkin Elmer-YGA7 instrument to obtain individual spectra. The thermogram records the percentage of weight

loss versus temperature. The mass change of the sample was recorded continuously over the temperature and time intervals. The weight loss of the samples was measured as a function of temperature. This method was described by Owolabi *et al*. (2017).

RESULTS AND DISCUSSION

Alkali Extraction

The yields of extracted hemicelluloses from OPEFB, which ranged between 23.0 to 29.5%, was in agreement with a similar report by Sun *et al*. (2000) that extracted hemicelluloses from rice straw. Alkaline-based hemicelluloses extraction is a result of cleavage of ester linkages between lignin and celluloses at the cell wall (Sun *et al*. 2004). In addition, the α-ether linkage between lignin and hemicelluloses is broken down by alkaline treatment (Palamae *et al*. 2014). Hemicelluloses can be extracted using potassium hydroxide (KOH) (Haliza *et al*. 2006); KOH favors the removal of hemicelluloses at higher concentration. Thus, NaOH is preferable as it removes lignin while minimizing the loss of hemicelluloses, which is desirable (Haliza *et al*. 2006).

Physical Characterization of Hemicelluloses Blend and Nanocomposite Films

Particle size measurement

The suspension of nanocellulose was subjected to zeta potential evaluation and had a mean value of -32.5 ± 1.5mV. The nanocellulose was considered stable because the absolute value of the zeta potential was higher than 25 mV (Chaturbhuj *et al*. 2016). The major particle size distribution was approximately 89.5 nm.

Film thickness and optical properties

Table 2 shows thickness and the optical properties (*i.e*., color), showing the Hunter (*L*, *a*, *b*) color values of nanocomposite films with the different ratios of hemicellulose and different CMC/MMT contents while the sample of the prepared films are shown in Fig 1. nanocomposite films were at least semitransparent by the virtue of the high *L* value. The film thickness is pivotal to the water permeability and mechanical properties.

Table 2. Thickness of Nanocomposite Hemicelluloses Films

Film	Thickness (mm)	Hunter color values		
		L (Transparency)	a (Redness/Greenness)	b (Yellowness/Blueness)
100CMC-MMT	0.1566 ± 1	97.61 ± 0.99	-3.3 ± 0.05	1.38 ± 0.09
20H-80CMC-MMT	0.1791 ± 2	0.08 ± 0.01	0.10 ± 0.04	2.74 ± 0.11
40H-60CMC-MMT	0.1821 ± 1	0.25 ± 0.02	0.28 ± 0.09	4.05 ± 0.12
60H-40CMC-MMT	0.2043 ± 2	0.08 ± 0.01	0.10 ± 0.04	7.61 ± 0.11
80H-20CMC-MMT	0.2191 ± 4	0.25 ± 0.02	0.28 ± 0.09	7.89 ± 0.13

The optical properties are very important in films meant for food packaging applications. The thickness of all nanocomposite films under investigations ranged between 0.16 and 0.22 mm while the MMT based pure films without hemicelluloses modification were translucent with the highest luminosity (*L*) value of 97.61 but decreased upon addition of hemicelluloses. Hence the incorporation of hemicelluloses fillers into the methyl cellulose matrix produced less translucent films compared with the MMT-CMC nanocomposite film.

The minor color changes of the nanocomposite films were visible due to the films with added MMT. As shown in Fig. 1, nanocomposite film without the hemicelluloses had better transparency than the blend film, which was because the MMT content of the films was well dispersed and therefore increased some transparency (Kanmani and Rhim 2014).

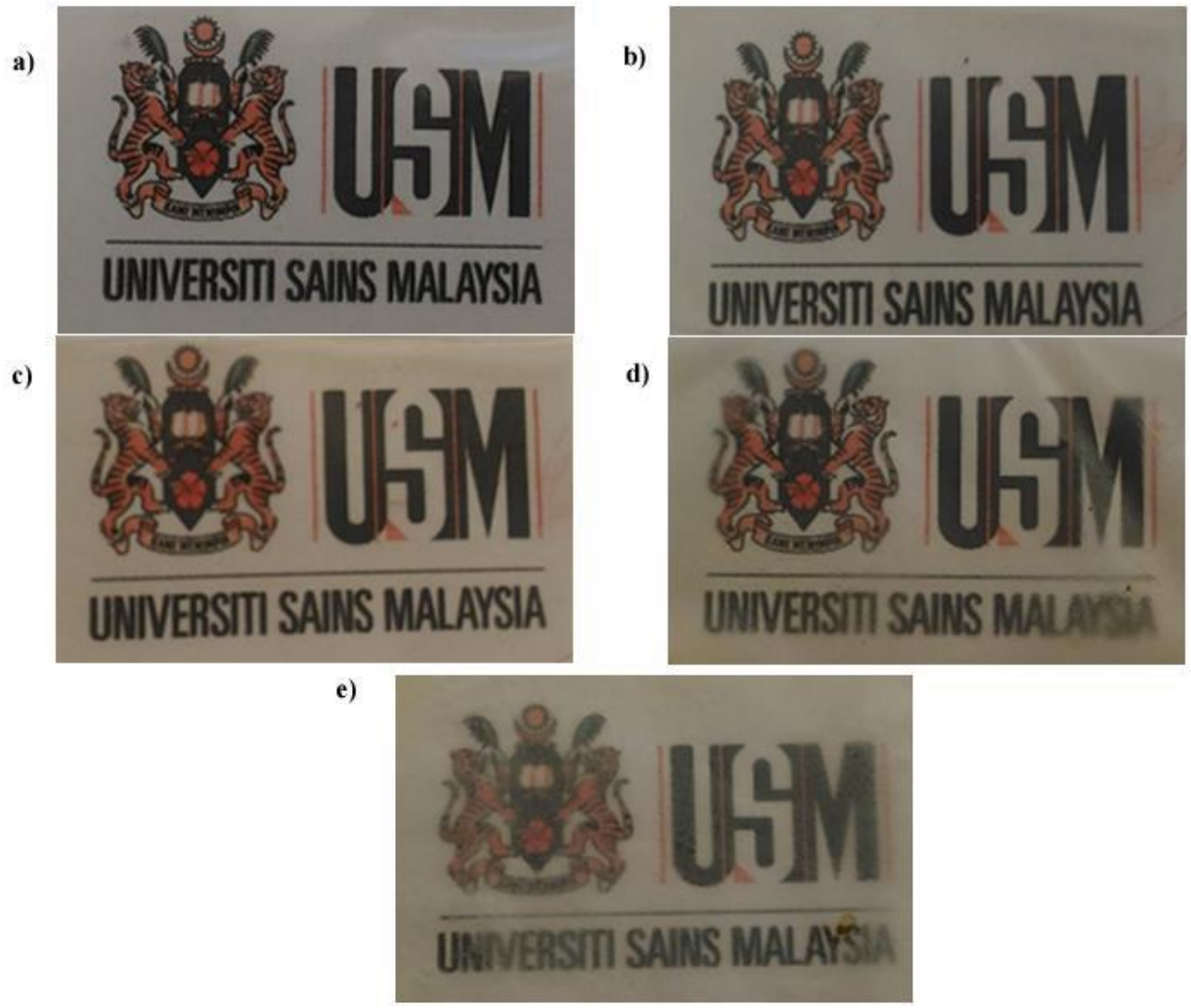

Fig. 1. Photographic images of (a) 100CMC-MMT (b) 20HMMT-80CMC, (c) 40HMMT-60CMC, (d) 60HMMT-40CMC and (e) 80HMMT-20CMC film

With an increase in ratio of hemicellulose to CMC/MMT, the *L*-value decreased, while *a*- and *b*-values increased. This result suggested that the introduction of the hemicellulose content directly affected the color of films. This could be attributed to the obstruction of visible wavelength by the increased addition of the hemicelluloses, leading to translucent or opaque films and decreasing the transparency of the films.

Wettability

Contact angles determination has been widely used to determine the wettability of a liquid on a solid surface. The rule of thumb for the study is that a high value of the contact angle θ indicates a higher cohesive strength within the bulk water hence a weak liquid-solid interaction therefore poor wetting. In contrast, low values of the contact angle θ, with spreading tendencies in solids showing strong liquid-solid interaction. The forces associated with the interaction of water with a surface are greater than the cohesive strength associated with bulk liquid water. The results of the contact angles for all films are shown in Fig. 2, with the highest contact angle of 87% for CMC- blended MMT/hemicellulose film. There were decreases in the contact angle to 54% with least additions of CMC. The highest contact angle recorded for 60HMMT-40CMC was as a result of enhanced hydrophobicity through the combination of blended MMT OPEFB hemicellulose with CMC film, which enhances the contact angle of the CMC- blended MMT/ hemicellulose blend.

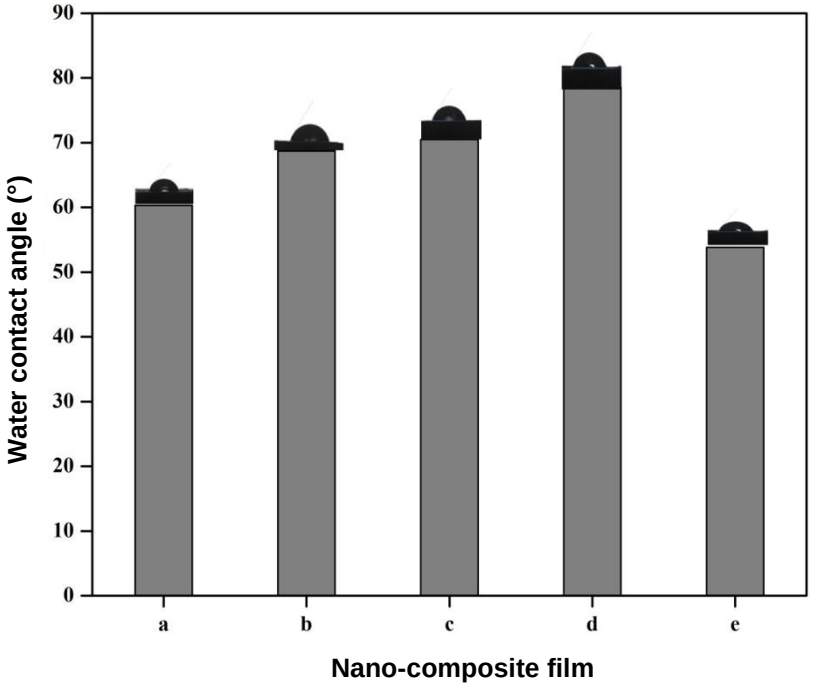

Fig. 2. Contact angle of nanocomposite films at (a) 100CMC-MMT, (b) 20HMMT-80CMC, (c) 40HMMT-60CMC, (d) 60HMMT-40CMC and (e) 80HMMT-CMC20

However, the lowest contact angle of 54% recorded for the combination of 80HMMT-CMC20 nanocomposite film could be attributable to the lowest value of the CMC in the nanocomposite formulation, resulting in least hydrophilic specimen. The results can be related to the theory of contact angle measurements, which predicts that if the values of contact angles are low, then the liquid will spread or wet well, while high values indicate poor wetting. This means that 80H-20CMC blend film had the least contact angle of 54% compared with others ratios.

As shown in Table 3, water vapor permeability decreased in the following order: 80H-20CMC > 20H-80CMC > 40H-60CMC > 60H-40CMC > 100CMC. Despite the modification of the CMC with the MMT, the WVP of the film increased with increased hemicelluloses blend due to many hydrophilic carboxyl groups. A similar trend was

reported by Bourtoom and Chinnan (2008). The incorporation of nanocellulose extracted from plant sources should improve the barrier properties of biocomposites because of its nanoscopic structure. However, hemicelluloses have relatively poor water vapor barrier characteristics, which result from their hydrophilicity; hence, high WVP of the nanocomposite film was observed as the proportion of hemicellulose increased (Asem *et al*. 2018). The moisture uptake is a crucial factor that determines the rate of degradation of a given product.

Table 3. Water Vapor Permeability of the Hemicelluloses Films

Hemicelluloses Film	Water Vapor Permeability(kg*am/m2*s*Pa)
100CMC-MMT	$1.075 \pm 0.08 \times 10^{-12}$
20H-80CMC-MMT	$1.150 \pm 0.12 \times 10^{-12}$
40H-60CMC-MMT	$1.110 \pm 0.15 \times 10^{-12}$
60H-40CMC-MMT	$1.057 \pm 0.21 \times 10^{-12}$
80H-20CMC-MMT	$1.220 \pm 0.11 \times 10^{-12}$

Physicochemical Analysis of the Biocomposite Films

The FTIR spectra of the MMT modified hemicelluloses-based nanocomposite films are shown in Fig. 3. The characteristic absorption of the modified hemicelluloses based groups are shown on the IR spectrum peak at 3516 and 3231 cm^{-1} and corresponded to the -OH stretching bond of the hemicellulose-based composite. The effect of hemicellulose loading in the nanocomposite was monitored in the fingerprint region by the appearance and disappearance of peaks. The new and strong absorption band at 2375 cm^{-1} confirmed the stretching vibration of the C-H stretching leading to strong compatibility of the composite at higher filler loading. Moreover, peaks at 1727 cm^{-1} and 1517 cm^{-1} attributed to carbonyl (C=O) and C=C stretching from CMC, respectively, but disappeared as the hemicellulose addition increased due to the intermolecular rearrangement.

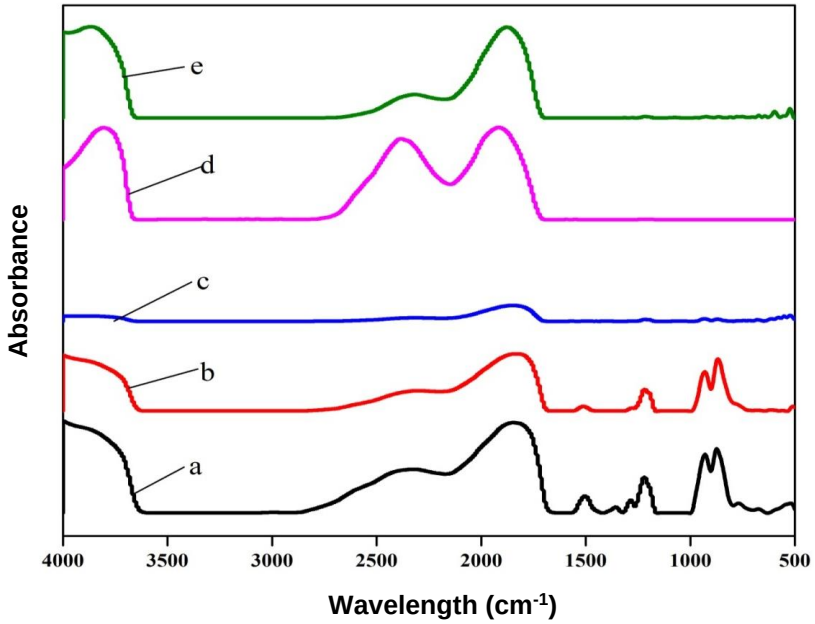

Fig. 3. FTIR spectra of nanocomposite films at (a) 100CMC-MMT, (b) 20HMMT-80CMC, (c) 40HMMT-60CMC, (d) 60HMMT-40CMC and (e) 80HMMT-CMC20

Peaks in the range of 1000 to 1150 cm^{-1} were C-O-C and C-O groups from carbohydrates in cellulose (Chen *et al*. 2016). These changes are attributable to a switch in the intramolecular hydroxyl-hydroxyl bonding to intermolecular hydroxyl-siloxane (Si-O-Si) hydrogen bonding. The peaks lost at 1500 cm^{-1} from film (c) to (e) indicated asymmetrical COO- stretching of CMC as the hemicelluloses loading increased. Moreover, the frequency of vibration band at 848 cm^{-1} assigned to the vibration of MMT - CMC, indicated Al-OH bonds formed strong hydrogen bonds *via* the hydroxyl groups of the hemicelluloses, and CMC interacted with Al on the clay platelet surface, as reported by Attaran *et al*. (2017).

The hydrogen bonds in the MMT-modified hemicelluloses based nanocomposite were strengthened, forming the strong interfacial attachment needed for stress transfer in 60HMMT-40CMC film. Similarly, the dual peak intensity peak appeared at 995 cm^{-1} (which later disappeared as the hemicelluloses loading increases), and the appearance of low intensity bands at 1700 to 1600 cm^{-1} were probably due to water present in the amorphous phase (Yeasmin and Mondal 2015). These changes of the IR spectra show the compatibility of both matrix and the filler components participated in the formation of the nanocomposite. Hence, the peak disappearance can be seen in Fig. 3.

X-ray Diffraction Analysis

The XRD pattern was performed to quantify the crystalline structure of hemicelluloses-based nanocomposite film as shown in Fig. 4. Composite film (a) shows a typical diffractogram of a CMC-MMT composite with broad diffraction peak at a 2θ =12.8°, 2θ = 20.44°, indicating partially crystalline character. CMC/MMT nanocomposite film with peaks at 2θ = 37.8° and at 38.12º, which decreases as the hemicelluloses loading increases from nanocomposite films (b-e). This is attributable to the fact that hemicellulose-based films are semicrystalline and hygroscopic. X-ray diffraction patterns of all the nanocomposite show weak peaks in the hemicelluloses-based nanocomposite films due to the amorphous nature of the hemicelluloses (Gu and Catchmark 2012). Generally, the peak exhibit different intensity from the pattern due to the number of hemicelluloses increased, the intensity of the peaks decreased.

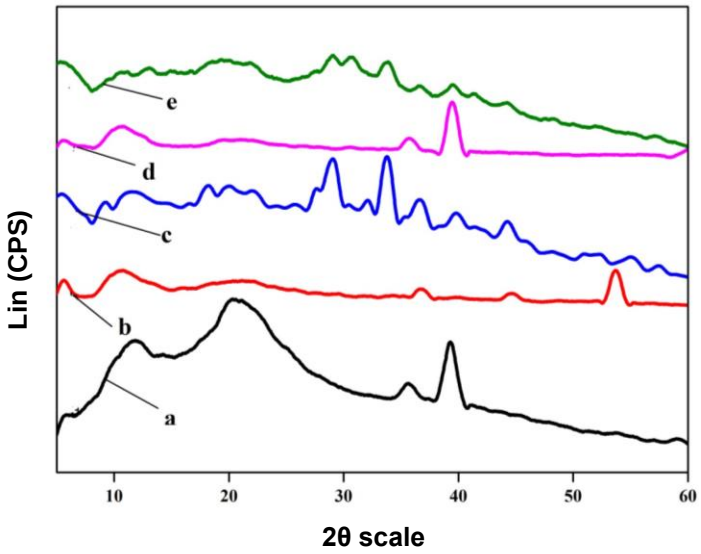

Fig. 4. X-ray diffractogram for all nanocomposite film; (a) 100CMC-MMT, (b) 20H-80CMC-MMT, (c) 40H-60CMC-MMT, (d) 60H-40CMC-MMT and (e) 80H-20CMC-MMT

The weak broad peak observed in all nanocomposites hemicelluloses film, suggested that the nano composite film were amorphous. The result further shows that the X-RD pattern of semi-crystalline structure at 2θ value of 39.0° for film (d) could be used to validate the highest tensile strength recorded for film 60H-40CMC-MMT, as discussed earlier. These results suggested that the crystalline structure which was mainly due to the addition of MMT polymer and explained the higher thermal temperature for film 60H-40CMC-MMT. Compatibility of the MMT-modified hemicelluloses-based nanocomposite has been seen from the results of the FTIR, and X-RD to increased strong hydrogen bonding, leading to improved tensile strength with the hemicelluloses loading through the great interaction between the two materials. On the other hand, the intensity of peaks decreased as the amount of hemicellulose increased. These results are in agreement with Migneault *et al*. (2015) and Adina *et al*. (2010). The disappearance of X-ray diffraction peaks corresponding to H-MMT-CMC films (a-e) confirms the interaction between two biopolymers. These results are supported by the work of Ju *et al*. (2015). This phenomenon illustrates the reduction hydrogen bonds between hydroxyls of the anhydroglucose units of cellulose.

Mechanical Properties of the Nanocomposite Films

The results for the mechanical properties investigated on the nanocomposite films, including the tensile strength, the tensile modulus, and the elongation at break are shown in Fig. 5.

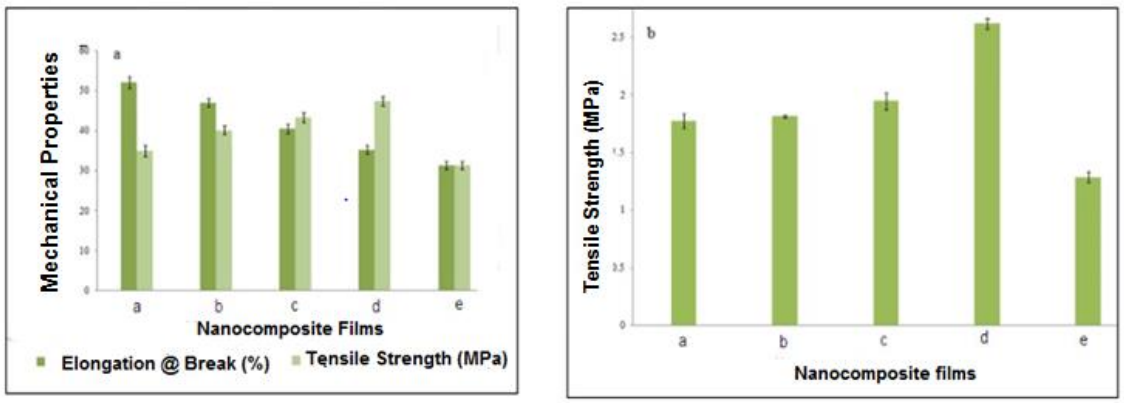

Fig. 5. Mechanical properties of the nanocomposite films. (a) Tensile strength and elongation at break; (b) tensile modulus. Within the panels, the samples are indicated by(a) 100CMC-MMT, (b) 20H-80CMC-MMT, (c) 40H-60CMC-MMT, (d) 60H-40CMC-MMT, and (e) 80H-20CMC-MMT

Regarding the mechanical properties of hemicelluloses-based films, hydrogen bond cross-linking happens at drying temperature in the oven (Palamae *et al*. 2017). This has a noticeable effect on the tensile strength and elongation of the films. There was an improvement in both the tensile strength and the tensile modulus with increased hemicelluloses loading up to 60H-40CMC-MMT, as indicated in Fig. 5. This is attributable to the increase in the electrostatic interactions resulting in the compatibility of the materials with the presence of MMT, which allowed good interfacial interaction. With 60H-40CMC-MMT loading, the tensile strength and tensile modulus reached the maximum value, which was 47.53 MPa and 2.62 MPa, respectively, as a result of good interaction between the filler and the matrix (Palamae *et al*. 2017). This interaction is an indication of strong electrostatic interactions, which allowed good interfacial interaction resulting in better

stress transfer between the filler particles and the matrix and consequently, enhanced the tensile strength of the composite. The addition of hemicelluloses up to 80% decreased the tensile strength of the nanocomposite film, which is an indication of poor adhesion between fiber and matrix due to the lack of transfer of stress from the matrix to the fiber material. Further increases in hemicelluloses loading resulted in a gradual decrease in the mechanical properties of the nanocomposite film. This is attributable to the inability of the 80H-20CMC-MMT nanocomposite film to transfer the load during tensile loading (Inácio *et al*. 2017), resulting in lower tensile strength and tensile modulus. This observation was in agreement with previous research on modifying hemicelluloses film (Chen *et al*. 2016). However, elongation at break of the composite film decreased with the increase in hemicelluloses loading.

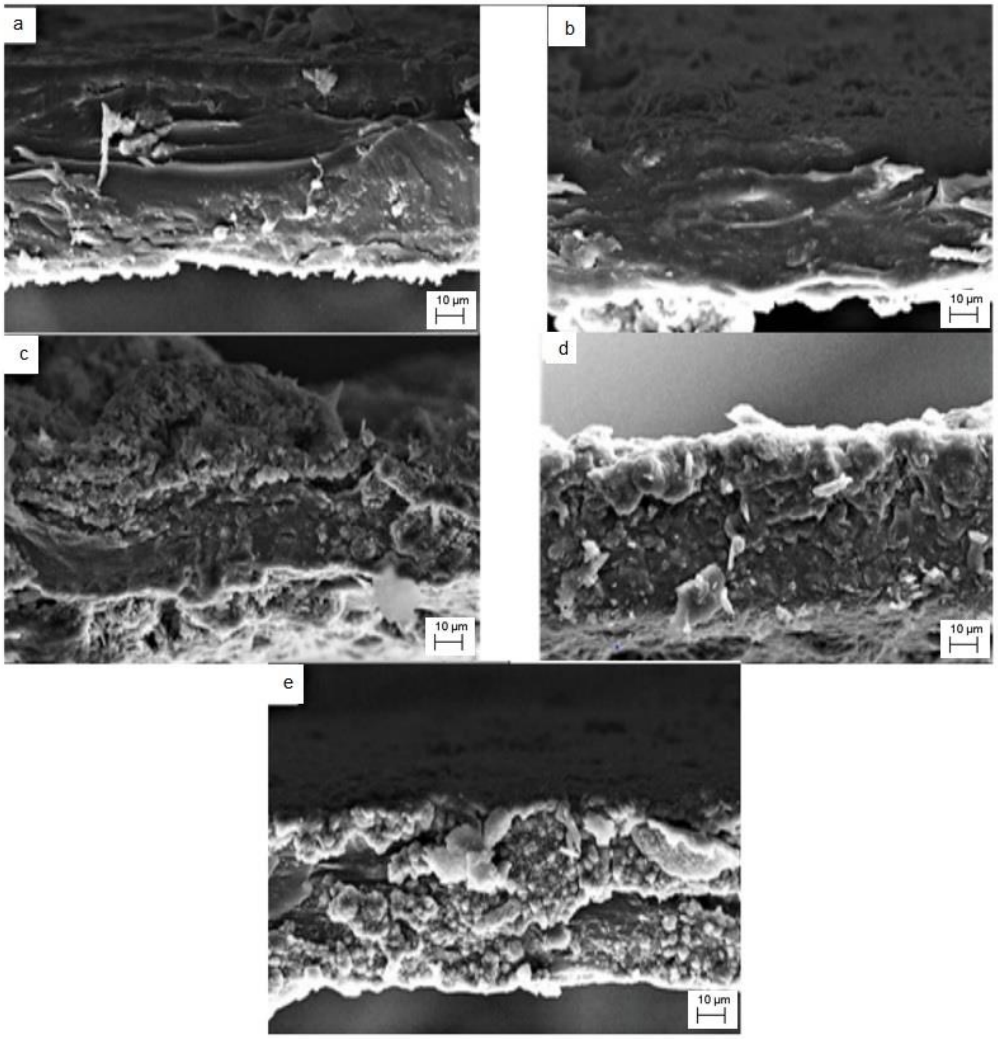

Fig. 6. Tensile fracture surface images of nanocomposite films; (a) 100CMC-MMT, (b) 20H-80CMC-MMT, (c) 40H-60CMC-MMT, (d) 60H-40CMC-MMT and (e) 80H-20CMC-MMT

The steady decreases in the elongation at break with increasing hemicellulose loading (Fig. 5a) is attributed to low elongation at break of natural fiber. Furthermore, the stiffness and brittleness of the nanocomposite as the hemicellulose load increased resulted in the decrease in elongation at break. This observation is similar to the a previous report (Inácio *et al*. 2017).

Scanning Electron Microscopy

SEM images of the nanocomposite at various hemicelluloses loadings are shown in Fig. 6 at 500× magnification. The images show very good dispersal of the filler in the matrix. The surface images show that despite the configuration, the filler-matrix materials contributed positively to the enhancement of the mechanical strength of the composite. The presence of MMT on the surface of hemicelluloses embedded with the CMC matrix improved the surface morphology of the CMC-MMT composite. The presence of MMT enhances the compatibility of the hemicelluloses fillers, which resulted in improved fiber matrix interface hence increased mechanical strength properties. Despite the lack of filler coagulations in the nanocomposite, the presence of interfacial fractures in the SEM image at the sample Film 80H-20CMC-MMT would have contributed to the mechanical strength failure resulting in the lowest value of both the tensile strength and tensile modulus.

Thermal Analysis

Differential scanning calorimetry (DSC)

DSC was used to study the phase transition of the hemicelluloses based biopolymer without any change in mass. DSC measures the heat flow with increasing temperature, with respect to the glass transaction temperature (T_g) and melting temperature (T_m) of the nanocomposite films. The DSC data were taken from the first heating cycle and is presented in Fig. 7.

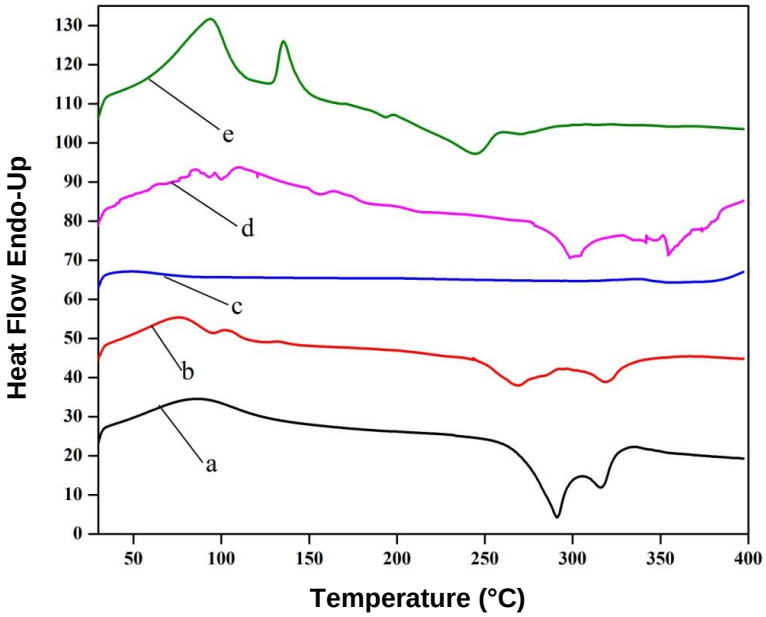

Fig. 7. DSC curve of all nanocomposite film; (a) 100CMC, (b) 20H-80CMC, (c) 40H-60CMC, (d) 60H-40CMC and (e) 80H-20CMC

The glass transition temperature (T_g) of the prepared nanocomposite was compared with other nano-composite films from different sources, as presented in Table 4. All samples showed a small endothermic peak at 100 °C, which was related to removal of moisture when the samples were heated. It reflects the hydrophilic nature of respective polymer (Inácio *et al*. 2018). The melting temperature T_m of native hemicelluloses was between 200 °C and 250 °C, but it changed upon hemicelluloses modification to between 250 °C and 290 °C. This is in line with a study by Stefani *et al*. (2005), which reported that

the lignocellulosic material decomposed thermochemically between 150 °C and 500 °C: hemicelluloses mainly between 150 °C and 350 °C, cellulose between 275 °C and 350 °C, and lignin between 250 °C and 500 °C.

Table 4. Comparison of the Glass Transition Temperature of Hemicellulose Films

Hemicellulose sources	T_g (ºC)	Reference
Beechwood	133	Moine *et al*. (2004)
Softwood kraft	158	Laine *et al*. (2016)
OPEFB	183 to 188	Measured

This change indicates good compatibility between the MMT-modified hemicelluloses based nanocomposite. However, at high hemicelluloses loading into the matrix, there was decreased film performance in terms of physical, mechanical, and thermal stability. The glass transition temperature (T_g) and the thermal degradation properties are important measures of polymers, as they can predict the thermal performance of the material. Theoretically, increased molecular weight or cross-linking increases the strength and the glass transition temperature of any given polymer (Palamae *et al*. 2017). It is therefore likely that the molecular weight of hemicelluloses affects the properties of the produced material. The DSC results showed an increase in the T_g value of 15 °C for the nanocomposite sample. The addition of MMT led to increased mechanical and thermal properties in hemicelluloses nanocomposite film. This could be due to two different reasons: (1) increased stability due to the increased molecular weight beyond the assumed molecular weight of the hemicelluloses and (2) linkages that are created between the aromatic units, causing reduced mobility of the polymer chains (Hassan and Badri 2016).

Thermogravimetric analysis

TGA measures the thermal stability of material by determining the mass loss with increasing temperature. Thermogravimetric analysis and the DTG profile of the nanopolymer films are shown in Figs. 8 and 9, respectively. Thermal stability can be expressed in the terms of the initial decomposition temperature (Wang *et al*. 2017), the temperature at onset of the decomposition, and residual content, as listed in Table 5 in conjunction with the result in Fig. 9.

Figure 8 shows the thermal stability of the nanocomposite obtained through TGA under nitrogen atmosphere. The first stage of decomposition, which is equivalent to 5% mass loss, was assigned to the evaporation of water (Garcia-Maraver *et al*. 2015). The temperature of 10% weight loss T_{10} of the films 100CMC-MMT, 20HMMT-80CMC, 40HMMT-60CMC, 60HMMT-40CMC, and 80HMMT-20CMC occurred at 243 °C, 246 °C, 248 °C, 254 °C, and 282 °C, respectively. These results are in accord with earlier reports on hemicellulose-based film of 283 °C from aspen wood (Liu *et al*. 2011), 292 °C from ryegrass leaves (Liu *et al*. 2006), and 228 °C from wheat straw (Azeredo *et al*. 2015). The thermal degradation temperatures (T_{20}%, T_{50}%), maximum degradation temperatures (T_{max}), and residual weight at 700 °C that corresponds to the char residue are listed in Table 5. Notably, the T_{max} of this study was between 300 and 304 °C, which was similar to Chen *et al*. (2016) with lesser residue at 700 °C. However, the hemicellulose-based film showed improvement in T_{max} compared with CMC-MMT film.

In the case of polymer nanocomposites, the improvement in thermal stability could be attributed to uniform dispersion of nanofiller in the matrix. A similar conclusion was drawn from other studies (Benhamou *et al*. 2015).

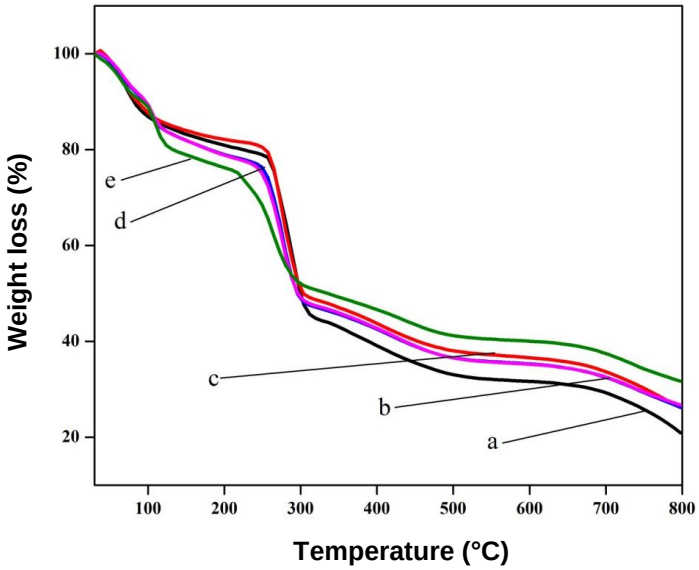

Fig. 8. TGA of nanocomposite films; (a) 100CMC-MMT, (b) 20HMMT-80CMC, (c) 40HMMT-60CMC, (d) 60HMMT-40CMC and (e) 80HMMT-20CMC

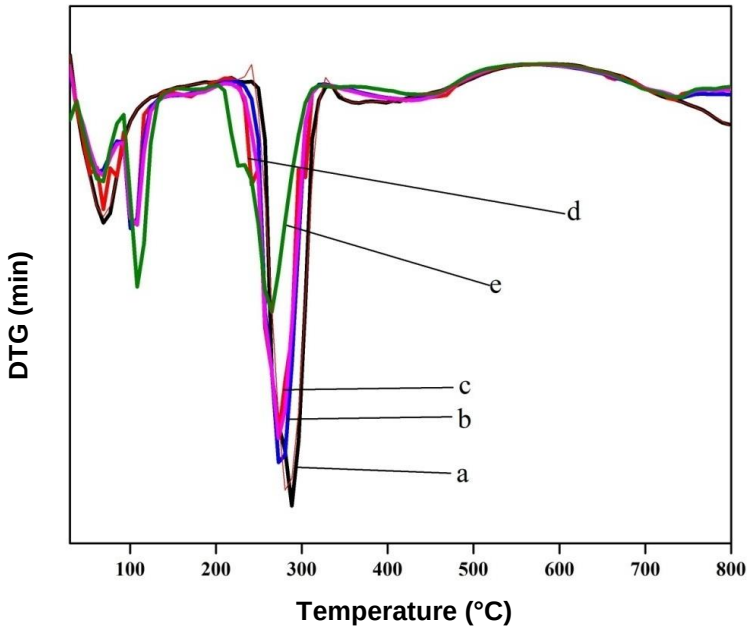

Fig. 9. DTG of nanocomposite films; (a) 100CMC, (b) 20H-80CMC, (c) 40H-60CMC, (d) 60H-40CMC and (e) 80H-20CMC

Table 5. Thermal Properties of Hemicelluloses Based Nanocomposite Films

Samples	Degradation Temperature (°C)			Residual Weight (%) at 700°C
	T_{20}	T_{50}	T_{max}	
100CMC	241	291	300	21.11
20H-80CMC	262	280	302	28.77
40H-60CMC	194	279	304	28.44
60H-40CMC	194	279	304	35.32
80H-20CMC	147	263	300	33.27

CONCLUSIONS

1. Eco-friendly nanocomposite films were successfully prepared from the combination of the CMC and premixed MMT/hemicellulose with particle size of 89.5 nm, resulting in good barrier properties for low to moderate relative humidity applications
2. The 60H-40CMC-MMT nanocomposite film gave the best physico-chemical, mechanical, thermal, and barrier properties, while greater hemicelluloses loading gave a poor result.
3. The SEM and FTIR studies confirmed the compatibility of the blended materials.
4. A uniform dispersion of fillers was expected for film 60H-40CMC-MMT due to the interlayer spacing of the MMT, leading to more intercalation, which in turn increased the tensile strength of the nanocomposites film.
5. The nanocomposite film showed high transparency, good thermal behavior, and poor water vapor permeability with the hemicelluloses loading.
6. The rate of weight loss was dependent on the hemicelluloses content, whereby the weight loss increased with additional hemicelluloses.
7. The result shows that the 2% MMT inclusion in the composite formulation was able to improve the functional properties of the hemicellulose-based nanocomposite films, hence reducing the water vapor permeability.

ACKNOWLEDGMENTS

The authors are thankful for the financial support provided by Universiti Sains Malaysia (USM) under Bridging Grant scheme (304.PTEKIND.6316255) and (304.PTEKIND.6316059).

REFERENCES CITED

Adina, C., Florinela, F., Abdelmoumen, T., and Carmen, S. (2010). "Application of FTIR spectroscopy for a rapid determination of some hydrolytic enzymes activity on sea buckthorn substrate," *Romanian Biotechnological Letters* 15(6), 5378-5744.

Aldaya, M. M., Allan, J. A., and Hoekstra, A. Y. (2010). "Strategic importance of green water in international crop trade," *Ecological Economics*, 69(4), 887–894.

DOI:10.1016/j.ecolecon.2009.11.001

Andberg, M., Maaheimo, H., Kumpula, E. P., Boer, H., Toivari, M., Penttilä, M., and Koivula, A. (2016). "Characterization of a unique *Caulobacter crescentus* aldose-aldose oxidoreductase having dual activities," *Applied Microbiology and Biotechnology* 100(2), 673-685.DOI: 10.1007/s00253-015-7011-5

Asem, M., Nawawi, W. M. F. W., and Jimat, D. N. (2018). "Evaluation of water absorption of polyvinyl alcohol-starch biocomposite reinforced with sugarcane bagasse nanofibre: Optimization using two-level factorial design," *IOP Conference Series: Materials Science and Engineering* 368(2018), 012005.DOI: 10.1088/1757-899X/368/1/012005

ASTM D882 (2000). "Annual book of ASTM standards," American Society for Testing and Materials, Philadelphia, PA, USA.

ASTM D570-98 (2002). "Annual book of ASTM standards," American Society for Testing and Materials, West Conshohocken, PA, USA.

ASTM D570-98 (2010). "Standard test method for water absorption of plastics," ASTM International, West Conshohocken, PA, USA.

Attaran, S. A., Hassan, A., and Wahit, M. U. (2017). "Materials for food packaging applications based on bio-based polymer nanocomposites," *Journal of Thermoplastic Composite Materials* 30(2), 143-173.DOI: 10.1177/0892705715588801

Azeredo, H. M. C., Kontou-Vrettou, C., Moates, G. K., Wellner, N., Cross, K., Pereira, P. H. F., and Waldron, K. W. (2015). "Wheat straw hemicellulose films as affected by citric acid," *Food Hydrocolloids* 50, 1-6. DOI: 10.1016/j.foodhyd.2015.04.005

Benhamou, K., Kaddami, H., Magnin, A., Dufresne, A., and Ahmad, A. (2015). "Bio-based polyurethane reinforced with cellulose nanofibers: A comprehensive investigation on the effect of interface," *Carbohydrate Polymers*122, 202-211.DOI: 10.1016/j.carbpol.2014.12.081

Bourtoom, T., and Chinnan, M. S. (2008). "Preparation and properties of rice starch-chitosan blend biodegradable film," *LWT - Food Science and Technology* 41(9), 1633-1641. DOI: 10.1016/j.lwt.2007.10.014

Chaker, A., Alila, S., Mutjé, P., Vilar, M. R., and Boufi, S. (2013). "Key role of the hemicellulose content and the cell morphology on the nanofibrillation effectiveness of cellulose pulps," *Cellulose* 20(6), 2863-2875. DOI: 10.1007/s10570-013-0036-y

Chaturbhuj, K. Saurabh, Asniza Mustapha, M. Mohd. Masri, A. F. Owolabi, M. I. Syakir, Rudi Dungani, M. T. Paridah, M. Jawaid, and Abdul Khalil, H. P. S. (2016). "Isolation and characterization of cellulose nanofibers from *Gigantochlo ascortechinii* as a reinforcement material," *Journal of Nanomaterials* 2016, Article ID 4024527, pp 1-8

Chen, G. G., Qi, X. M., Guan, Y., Peng, F., Yao, C. L., and Sun, R. C. (2016). "High strength hemicellulose-based nanocomposite film for food packaging applications," *ACS Sustainable Chemistry and Engineering* 4(4), 1985-1993. DOI: 10.1021/acssuschemeng.5b01252

Creighton, M. A., Zhu, W., Van Krieken, F., Petteruti, R. A., Gao, H., and Hurt, R. H. (2016). "Three-dimensional graphene-based microbarriers for controlling release and reactivity in colloidal liquid phases," *ACS Nano* 10(2), 2268-2276. DOI: 10.1021/acsnano.5b06963

Garcia-Maraver, A., Perez-Jimenez, J. A., Serrano-Bernardo, F., and Zamorano, M. (2015). "Determination and comparison of combustion kinetics parameters of agricultural biomass from olive trees," *Renewable Energy*83(C), 897-904. DOI:

10.1016/j.renene.2015.05.049
Gu, J., and Catchmark, J. M. (2012). "Impact of hemicelluloses and pectin on sphere-like bacterial cellulose assembly," *Carbohydrate Polymers* 88(2), 547-557. DOI: 10.1016/j.carbpol.2011.12.040
Haliza, A. H. N., Fazilah, A., and Azemi, M. N. (2006). "Development of hemicelluloses biodegradable films from oil palm frond (*Elaeis guineensis*)," in: *International Conference on Green and Sustainable Innovation*, Chiang Mai, Thailand, pp. 145.
Hassan, N. S., and Badri, K. (2016). "Thermal behaviors of oil palm empty fruit bunch fiber upon exposure to acid-base aqueous solutions," *Malaysian Journal of Analytical Sciences* 20(5), 1095-1103.DOI: 10.17576/mjas-2016-2005-15
Inácio, A. L. N., Nonato, R. C., and Bonse, B. C. (2017). "Recycled PP/EPDM/talc reinforced with bamboo fiber: Assessment of fiber and compatibilizer content on properties using factorial design," *Polymer Testing* 61, 214-222. DOI: 10.1016/j.polymertesting.2017.05.022
Inácio, A. L. N., Nonato, R. C., and Bonse, B. C. (2018). "Mechanical and thermal behavior of aged composites of recycled PP/EPDM/talc reinforced with bamboo fiber," *Polymer Testing*72, 357-363. DOI: 10.1016/j.polymertesting.2018.10.035
Jouki, M., Yazdi, F. T., Mortavazi, S. A., and Koocheki, A. (2013). "Physical, barrier and antioxidant properties of a novel plasticized edible film from quince seed mucilage," *International Journal of Biological Macromolecules* 62, 500-507. DOI:10.1016/j.ijbiomac.2013.09.031.
Ju, X., Bowden, M., Brown, E. E., and Zhang, X. (2015). "An improved X-ray diffraction method for cellulose crystallinity measurement," *Carbohydrate Polymers*123, 476-481. DOI: 10.1016/j.carbpol.2014.12.071
Kanmani, P., and Rhim, J. W. (2014). "Properties and characterization of bionanocomposite films prepared with various biopolymers and ZnO nanoparticles," *Carbohydrate Polymers*106, 190-199.DOI: 10.1016/j.carbpol.2014.02.007
Liu, C. F., Xu, F., Sun, J. X., Ren, J. L., Curling, S., Sun, R. C., Fowler, P., and Baird, M. S. (2006). "Physicochemical characterization of cellulose from perennial ryegrass leaves (*Lolium perenne*)," *Carbohydrate Researc*h 341(16), 2677-2687. DOI: 10.1016/j.carres.2006.07.008
Liu, W., Yuan, Z., Mao, C., Hou, Q., and Li, K. (2011). "Removal of hemicelluloses by NaOH pre-extraction from aspen chips prior to mechanical pulping," *BioResources* 6(3), 3469-3480. DOI: 10.15376/biores.6.3.3469-3480
Luqueta, G. R., Dos Santos, E. D., Pessoa, R. S., and Maciel, H. S. (2017). "Evaluation of disposable medical device packaging materials under ozone sterilization," *Revista Brasileira de Engenharia Biomedica* 33(1), 58-68. DOI: 10.1590/2446-4740.03216
Makwana, D., Castaño, J., Somani, R. S., and Bajaj, H. C. (2018). "Characterization of Agar-CMC/Ag-MMT nanocomposite and evaluation of antibacterial and mechanical properties for packaging applications," *Arabian Journal of Chemistry*. DOI: 10.1016/j.arabjc.2018.08.017
Migneault, S., Koubaa, A., Perré, P., and Riedl, B. (2015). "Effects of wood fiber surface chemistry on strength of wood-plastic composites," *Applied Surface Science*343, 11-18. DOI: 10.1016/j.apsusc.2015.03.010
Nasrabadi, T., Mottaghifar, H., and Pourasghar, F. (2017). "Life cycle assessment towards optimization of water use in an industrial cattle farming complex by focusing on virtual water approach (case study: Foka complex)," *Journal of Environmental Studies* 42(4), 719-733. DOI: 10.22059/JES.2017.60937

Owolabi, A. F., Haafiz, M. K. M., Hossain, M. S., Hussin, M. H., and Fazita, M. R. N. (2017). "Influence of alkaline hydrogen peroxide pre-hydrolysis on the isolation of microcrystalline cellulose from oil palm fronds," *International Journal of Biological Macromolecules* 95, 1228-1234.DOI: 10.1016/j.ijbiomac.2016.11.016

Palamae, S., Dechatiwongse, P., Choorit, W., Chisti, Y., and Prasertsan, P. (2017). "Cellulose and hemicellulose recovery from oil palm empty fruit bunch (EFB) fibers and production of sugars from the fibers," *Carbohydrate Polymers*155, 491-497.DOI: 10.1016/j.carbpol.2016.09.004

Palamae, S., Palachum, W., Chisti, Y., and Choorit, W. (2014). "Retention of hemicellulose during delignification of oil palm empty fruit bunch (EFB) fiber with peracetic acid and alkaline peroxide," *Biomass and Bioenergy*66, 240-248. DOI: 10.1016/j.biombioe.2014.03.045

Reza, M. T., Yan, W., Uddin, M. H., Lynam, J. G., Hoekman, S. K., Coronella, C. J., and Vásquez, V. R. (2013). "Reaction kinetics of hydrothermal carbonization of loblolly pine," *Bioresource Technology* 139, 161-169. DOI: 10.1016/j.biortech.2013.04.028

Stefani, P. M., Garcia, D., Lopez, J., and Jimenez, A. (2005). "Thermogravimetric analysis of composites obtained from sintering of rice husk-scrap tire mixtures," *Journal of Thermal Analysis and Calorimetry* 81(2), 315-320. DOI: 10.1007/s10973-005-0785-4

Sun, J. X., Mao, F. C., Sun, X. F., and Sun, R. C. (2004). "Comparative study of hemicelluloses isolated with alkaline peroxide from lignocellulosic materials," *Journal of Wood Chemistry and Technology* 24(3), 239-262.DOI: 10.1081/WCT-200038170

Sun, R. C., Tomkinson, J., Ma, P. L., and Liang, S. F. (2000). "Comparative study of hemicelluloses from rice straw by alkali and hydrogen peroxide treatments," *Carbohydrate Polymers* 42(2), 111-122. DOI: 10.1016/S0144-8617(99)00136-8

Wang, Q., Hisatomi, T., Suzuki, Y., Pan, Z., Seo, J., Katayama, M., Minegishi, T., Nishiyama, H., Takata, T., Seki, K., Kudo, A., Yamada, T., and Domen, K. (2017). "Particulate photocatalyst sheets based on carbon conductor layer for efficient Z-scheme pure-water splitting at ambient pressure," *Journal of the American Chemical Society* 139(4), 1675-1683. DOI: 10.1021/jacs.6b12164

Wanrosli, W. D., Zainuddin, Z., and Lee, L. K. (2004). "Influence of pulping variables on the properties of *Elaeis guineensis* soda pulp as evaluated by response surface methodology," *Wood Science and Technology* 38(3), 191-205. DOI: 10.1007/s00226-004-0227-7

Yeasmin, M. S., and Mondal, M. I. H. (2015). "Synthesis of highly substituted carboxymethyl cellulose depending on cellulose particle size," *International Journal of Biological Macromolecules* 80, 725-731. DOI: 10.1016/j.ijbiomac.2015.07.040

Yu, W. X., Wang, Z. W., Hu, C. Y., and Wang, L. (2014). "Properties of low methoxyl pectin-carboxymethyl cellulose based on montmorillonite nanocomposite films," *International Journal of Food Science and Technology* 49(12), 2592-2601. DOI: 10.1111/ijfs.12590

Article submitted: March 5, 2019; Peer review completed: June 16, 2019; Revised version received: June 28, 2019; Accepted: June 30, 2019; Published: August 21, 2019.
DOI: 10.15376/biores.14.4.8029-8047